Phase-lead reconstruction of a photoelastic tactile sensor

R. E. Saad
Department of Electrical & Computer Engineering

A. Bonen
Department of Electrical & Computer Engineering

K. C. Smith
Department of Electrical & Computer Engineering

B. Benhabib*
Department of Mechanical Engineering

Computer Integrated Manufacturing Laboratory, University of Toronto
5 King's College Road, Toronto, Ontario, Canada M5S 1A4
*beno@me.utoronto.ca

ABSTRACT

In this paper, a novel tactile photoelastic transducer for normal forces is presented. When a normal input force profile is applied to the transduction medium, stress is generated in the photoelastic layer making it birefringent. Consequently, circularly-polarized input light becomes elliptically polarized at the output due to the introduction of a phase-lead distribution. If a circular-reflection polaridoscope is used, the output light-intensity is a circular function of the total phase-lead distribution.

The first part of the paper describes the forward analysis of the transducer using finite-element analysis to determine the stress distribution in the transducer. Then, the phase-lead distribution is determined using the theory of photoelasticity. The second part of the paper describes a technique for the recovery of the phase-lead distribution from the ideal noise-free light-intensity distribution. Also, a verification method is proposed to determine whether a recovered phase-lead distribution is the correct one or not.

In the third part of the paper, we consider the non-ideal situation, where the light-intensity distribution is no longer noise-free. Quantization errors added to the detected light-intensity distribution are also considered. Recovering the phase-lead distribution under noisy conditions constitutes an ill-posed inverse problem. An algorithm that accurately and effectively determines the phase-lead distribution from a noisy light-intensity distribution is presented. The inverse-tactile problem is solved using an optimization function.

Keywords: tactile sensing, ill-posed problem, inverse problem, photoelasticity.

1. INTRODUCTION

Among the required sensory capabilities of future robots are those related to physical contact with the external environment. Explorations of diverse technologies that can possibly be associated with tactile sensing have resulted in the utilization of several forms of force transduction. Among the common methods of transduction are piezoelectric, piezoresistive, capacitive and optical. Extensive surveys of robotic-tactile-transduction technologies, providing considerable details of the performance of each of these types of tactile sensors, have been presented in several works.[1-3]

Amongst optical methods, there exists a strong possibility that photoelastic tactile sensors could be implemented in the near future using integrated optics and optoelectronics, in a manner analogous to piezoresistive tactile transducers that are presently implemented using micromachining and microelectronics.[4]

The few studies that have been published on photoelastic tactile sensors include the description,[5] an implementation of a basic sensor,[6] and a theoretical model used to analyze it.[7] Research results presented in these papers clearly show that a photoelastic transducer can satisfy many of the tactile-sensing requirements specified by Harmon.[8] In an earlier work,[9] although the researchers were successful in developing a photoelastic contact sensor, their transducer cannot be adapted directly for tactile sensing.

Photoelastic sensors have also been developed to detect slippage. One such sensor[10] uses a transducer similar to the one used for tactile sensing,[5,6] however, in this case, direct analysis of the fringes is used to detect movement of the grasped object: a special technique was reported to optimize the comparison process for detecting differences between two fringe patterns occurring due to the slippage of the grasped object.[11]

All of the photoelastic sensors developed thus far for robotics use a polaridoscope for illuminating and collecting the light from the photoelastic transducer. Polaridoscopes can be either linear or circular depending on the required polarization of the light. Also they can be characterized as reflective or transparent depending on whether the photoelastic transducer reflects or transmits the light.[12]

A circular reflective polaridoscope is shown in Figure 1. The input light is linearly polarized and then directed toward the photoelastic transducer by a beam splitter. Before reaching the transducer the light is circularly polarized by a quarter-wave plate. Once the light

penetrates the transducer, its polarization is affected by the birefringence induced in the photoelastic element by the forces applied to the transducer. The birefringence creates a phase-lead distribution that transforms the circularly-polarized light into elliptically-polarized light. A reflecting surface on the back side of the transducer returns the light toward a detector through the quarter-wave plate, the beam splitter and an analyzer. The output light-intensity distribution consists of a fringe pattern, as will be discussed in Section 2.

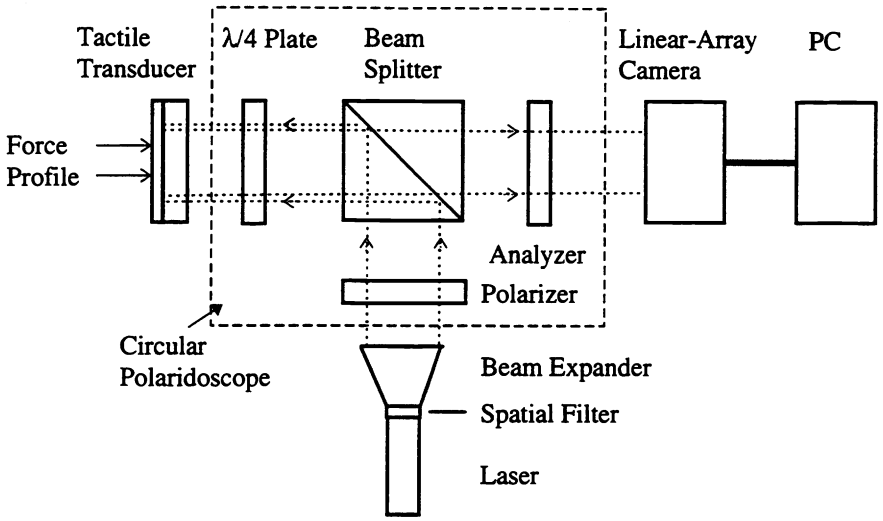

Fig. 1. A circular reflective polaridoscope.

The photoelastic tactile transducer developed in our laboratory consists of a simply-supported two-layer beam, with a mirrored surface between the two layers, Fig. 2.[13,14] In our analysis, it is assumed that normal line-distributed forces, separated by equal distances, *s*, from each other, are applied to part of the top surface of the beam. The area covered by these lines is referred to as the force-application region. The upper compliant layer is added to protect the rear surface of the mirror. For simplicity, it is assumed that this layer has the same mechanical properties as the lower photoelastic layer.

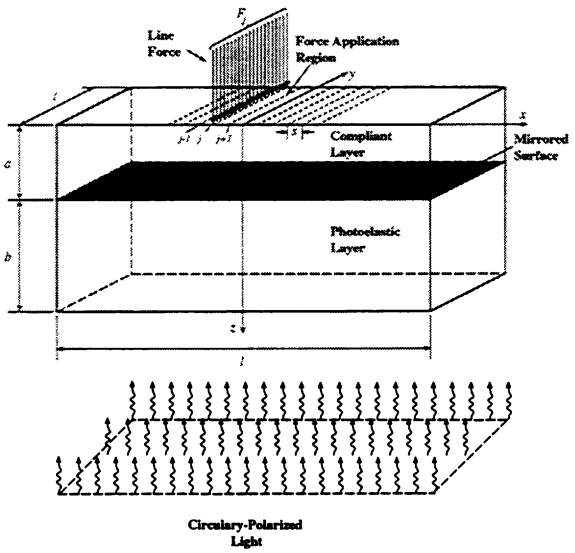

Fig. 2. Photoelastic tactile transducer under study.

Circularly-polarized monochromatic light illuminates the bottom surface of the transducer. A circular-reflection polaridoscope is used for this purpose. The light propagates parallel to the *z*-axis, passes through the photoelastic material, reflects from the mirror, and returns through the photoelastic material. If no force is applied onto the transducer, the returning light is circularly polarized since the photoelastic

material is isotropic. If a force profile is applied, stresses are induced in the photoelastic layer making the material birefringent. This introduces a certain phase-difference (a phase-lead) between the components of the electric field associated with the light-wave propagation in the two allowed directions of polarization.[15] The two directions of polarization are in the plane perpendicular to the direction of propagation, in our case the x-y plane. As a consequence of this effect, the output light is elliptically polarized, creating a phase-lead distribution, p, between the input light and the output light.

In Section 2, finite-element analysis (FEA) is used to calculate the stress distribution in the photoelastic transducer when forces are applied to it. Combining the theory of photoelasticity and the stresses previously determined, the phase-lead distribution can be calculated. The calculation of stresses using FEA rather than relying on approximate closed-form equations,[16] has been proposed in several recent works aimed at motivating better models for the increasing complexity of evolving transducers.[17-19] The analysis presented in Section 2 corresponds to the forward analysis of the tactile sensor.

In Section 3, the basic inverse problem in sensing. is described. It consists of recovering the phase-lead distribution (a linear function of the force profile) from the (ideal) noise-free light-intensity. Also in this section a method is presented by which to verify if a recovered phase-lead is correct or not.

In Section 4, the non-ideal case is addressed. It is assumed that the light-intensity is detected by a CCD camera linked to an A/D converter. Both elements introduce electronic noise, and the A/D converter adds quantization error to the detected light-intensity distribution, such that the inverse problem of recovering the phase-lead distribution from the light-intensity distribution becomes an ill-posed problem. To overcome the ill-posedness of the problem, an algorithm consisting of two major steps is presented: The first step consists of reducing the space of possible solutions, taking into account a series of verification rules, based on some expected behavior of the solution, that includes the verification of the boundary conditions of the problem. The second step consists of finding the correct solution amongst the reduced space of possible solutions. This step depends strongly on some known physical properties of the solution, and on the fact that the final solution can only be a linear combination of some pre-established functions.

2. FINITE-ELEMENT STRESS ANALYSIS OF THE TRANSDUCER

The calculation of the induced phase-lead distribution can be done using the photoelastic law that links the stress distribution to the phase-lead distribution.[12] In our case, the phase-lead distribution $p(x)$ can be calculated by:[7]

$$p(x)=2K_t\int_a^{a+b}\sigma_x(x,z)dz\,, \tag{1}$$

where K_t is a constant and σ_x is the stress along the x-axis. In this equation, it is assumed that the stresses are cylindrical along the y-axis, since the forces in each tactel of the transducer are applied along the y-axis. The constant K_t is given by:

$$K_t=\frac{1+\nu_2}{E_2}K_s\frac{2\pi}{\lambda}\,, \tag{2}$$

where λ is the wavelength of the light, ν_2 and E_2 are the Poisson's coefficient and the modulus of elasticity of the photoelastic layer, respectively, and K_s is the photoelastic strain constant.

The calculation of the 2-D distribution of stresses in the photoelastic transducer is carried out using FEA. The first step in calculating the stresses consists of establishing a mesh characterizing the photoelastic transducer, Fig. 3. In our case, the central part of the mesh has more elements than the outer parts in order to improve the accuracy of the stress calculations in the central region where the forces are applied. For the FEA example presented in this paper, the number of elements of the mesh is 5,025 (201×25), the maximum allowed by the software used (ANSYS -academic version) for the geometry of the elements used in this analysis. It is also assumed that the compliant layer and the photoelastic material have the same mechanical properties (the same modulus of elasticity and the same Poisson's coefficient), the materials of both layers work in the linear-elastic region and the forces are applied only at the tactels (See Fig. 2). Finally, it is assumed that the transducer is supported only at the bottom. As a consequence of these boundary conditions, Elasticity Theory establishes that the stresses must be zero at $x=-l/2$ and $x=l/2$. Due to numerical errors, stresses would not be zero, but actually be very small. For the analysis at hand, plane-stress conditions are assumed as well.[3]

Since stresses are calculated by the FEA at each of the nodes of the mesh, Equation (1) is re-written as:

$$p(x_i)=2K\sum_{N_i}\sigma_x(x_i,z_i)\Delta z_2\,, \tag{3}$$

where $\sigma_x(x_i, z_i)$ is the stress at the coordinates (x_i, z_i), Δz_2 is the length between two consecutive nodes along the z-axis in the photoelastic layer and N_i is the set of nodes in the photoelastic layer at a fixed x_i coordinate.

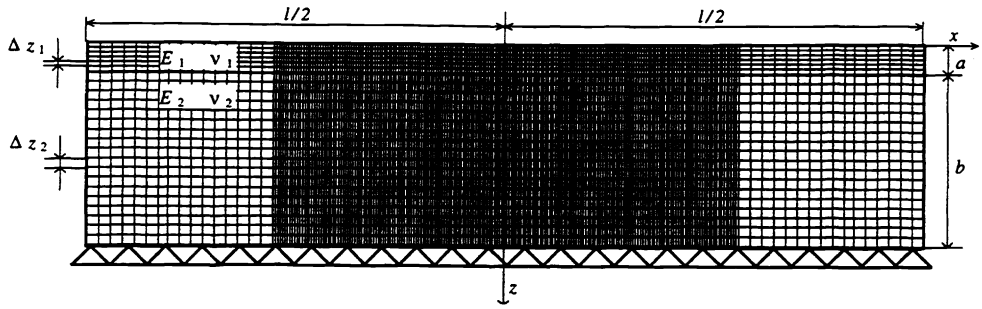

Figure 3: Finite element mesh representation for the transducer.

Suppose, as an example, that the force profile shown in Fig. 4 is applied to the transducer defined in Table 1. After calculating the stress distribution using FEA and applying (3), the resulting phase-lead distribution is as shown in Fig. 5. The continuous line in Fig. 5 represents a linear interpolation of the 201 consecutive points.

Table I: Dimensions and parameters of the sensor.

l	t	a	b	$E_1=E_2$	$\nu_1=\nu_2$	λ	K_s	s	N_t
25 mm	2 mm	0.5 mm	3 mm	0.0046 GPa	0.49	632.8 nm	0.009	1 mm	11

Applying the principle of superposition to stresses, one can easily prove that the phase-lead distribution can be re-written as:

$$p(x_i)=\frac{1}{W}\sum_{j=1}^{N_t}\psi_j(x_i)F_j\,, \tag{4}$$

where ψ_j are the complete set of the corresponding phase-lead distributions when a load W is applied at the j^{th} tactel, F_j is the magnitude of the force and N_t is the number of tactels. The family of ψ functions completely characterizes the transducer since, if they are known, the phase-lead distribution corresponding to any force profile can be obtained by applying (4). The family of ψ functions are linearly independent in the interval $I=[-l/2\ l/2]$. For clarity only some of the functions of the family (for W=0.4 N) are shown in Fig. 6.

The phase-lead distribution induced in the photoelastic material produces a light-intensity distribution at the output of the polaridoscope that is given by:

$$I(x)=\sin^2\frac{p(x)}{2}. \tag{5}$$

Fig. 7 shows the light-intensity distribution corresponding to the phase-lead distribution of our example. This completes the forward analysis of the transducer.

3. PHASE-LEAD DISTRIBUTION RECOVERY

Prior to the study of the non-ideal case, it is beneficial to determine how to recover the phase-lead distribution from a noise-free *continuous* light-intensity distribution. The study of this simpler case will show us some of the possible causes for the ill-posed conditions introduced by noise and discretization.

Let Equation (5) be inverted as:

$$\tilde{p}(x)=-2\arcsin\sqrt{I(x)}\,, \tag{6}$$

where $\tilde{p}(x)$ is the recovered phase-lead distribution. In this equation, it is assumed that the phase-lead distribution will always be negative or eventually zero, when the light-intensity is zero. Note that the phase-lead distributions ψ_i are negative (except at a few points where they could be zero) and the forces F_i are positive since only compression is allowed. In Figure 8, the recovered phase-lead distributions $\tilde{p}(x)$ and $p(x)$ are shown. For this case, it is clear that $\tilde{p}(x)$ is not the correct phase-lead based on given knowledge of the correct distribution. In practice however, the phase-lead distribution $p(x)$ would not be known a priori. Then, an important issue that must be addressed is whether one can identify an efficient means by which to determine that in our example $\tilde{p}(x)$ is not the sought phase-lead distribution.

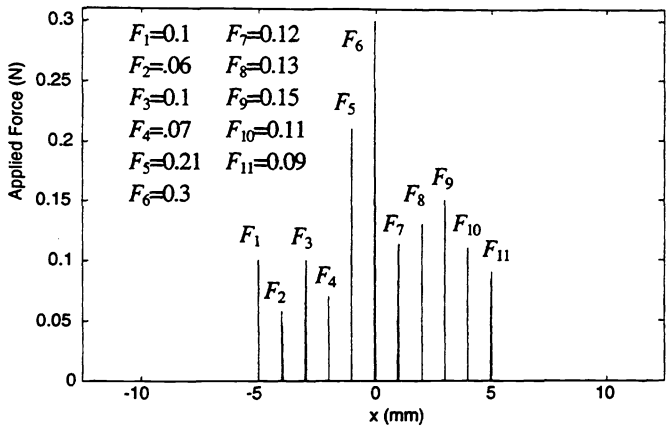

Fig. 4. Applied force profile.

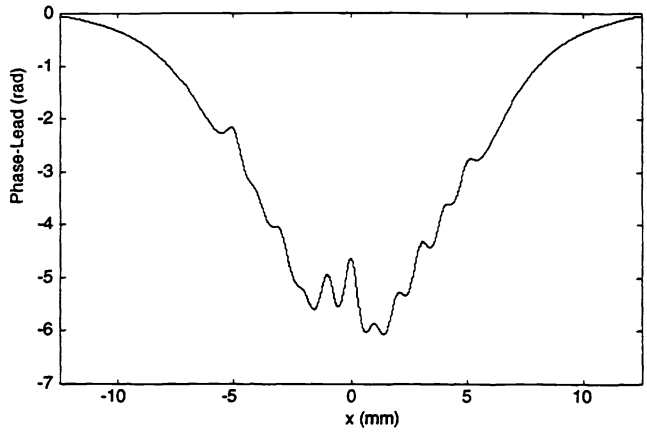

Fig. 5. Phase-lead distribution for the example.

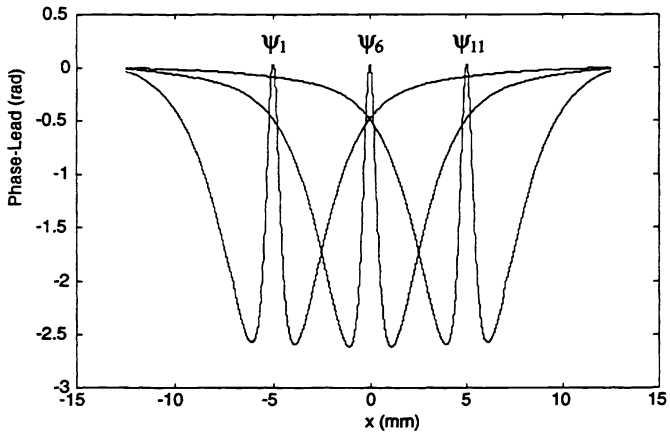

Fig. 6. Some of the phase-lead distributions.

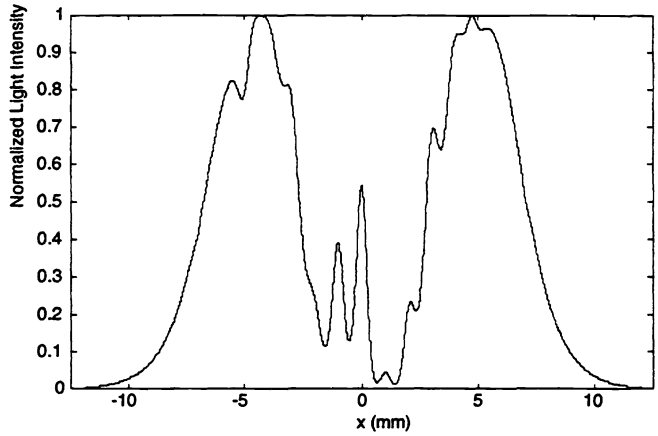

Fig. 7. Normalized light-intensity distribution.

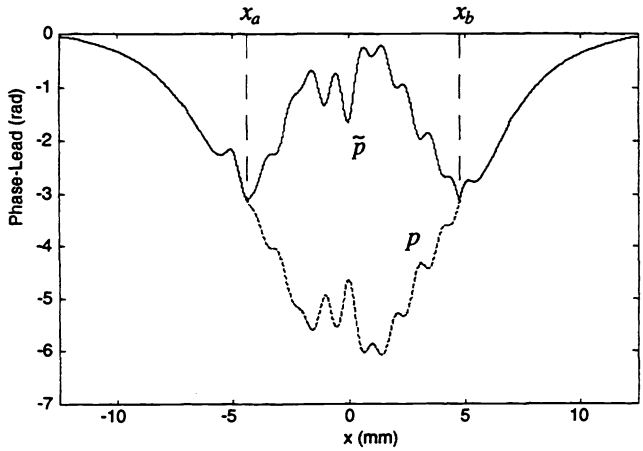

Fig. 8. Phase-lead distributions $\tilde{p}(x)$ and $p(x)$.

3.1. Proposed Verification Method

The recovered phase-lead distribution must satisfy (4), otherwise the phase-lead distribution is incorrect. In Appendix I, it is proven that when $p(x)$ is smaller than $-\pi$ in the interval I, the corresponding $\tilde{p}(x)$ obtained by (6) is not a linear combination of the ψ functions, assuming that the ψ functions are linearly independent in any open sub-interval of I. An alternative approach to showing that $\tilde{p}(x)$ is not a linear combination of the ψ functions can be explained assuming that the ψ functions have continuous derivatives in I. In that case, if $\tilde{p}(x)$ is a linear combination of the ψ functions, the derivative of $\tilde{p}(x)$ in the interval I should be continuous. Since the derivative of $\tilde{p}(x)$ in the interval I is not continuous, $\tilde{p}(x)$ is not a linear combination of the phase-lead distribution. Note that for $x = x_a$ and $x = x_b$, $\tilde{p}(x)$ has discontinuous derivatives. In Appendix I, the proof is more generic and does not require either that the ψ functions have continuous derivatives in I, or that $\tilde{p}(x)$ be discontinuous in I.

This result can be used to decide if a recovered phase-lead distribution is (or is not) the correct phase-lead distribution: *If the recovered phase-lead is a linear combination of the family of ψ functions in I, then the recovered phase-lead distribution is the correct one, otherwise it is incorrect.*

This conclusion constitutes the basis of the algorithm detailed in the following section.

3.2. Recovery of the phase-lead distribution by a full analytical study of the light-intensity distribution

The proposed method allows the recovery of the phase-lead distribution by a full analysis of the light-intensity distribution. The disadvantage of applying this method is the necessity for the calculation of high-order derivatives at critical points.[13]

Differentiating (5) yields:

$$\frac{dI}{dx}(x)=\frac{1}{2}\sin p(x)\frac{dp}{dx}(x). \tag{7}$$

The critical points of $I(x)$ can be found by analyzing $\frac{dI}{dx}=0$, namely where

$$\sin p(x)=0, \tag{8.a}$$

or/and

$$\frac{dp}{dx}(x)=0. \tag{8.b}$$

Equation (8.a) simply indicates that the phase-lead is zero or a multiple of π, and (8.b) determines the critical point of $p(x)$. It should be noted that some critical points can satisfy (8.a) and (8.b) simultaneously. These particular points are the ones that complicate the recovery of the phase-lead distribution.

The following algorithm is an analytical method for the recovery of a general phase-lead distribution from the normalized light-intensity distribution. A detailed explanation of the algorithm has been previously reported.[13]

The first step in the algorithm is the classification of the critical points of $I(x)$ as follows:

(a) *Class 1*: critical points of $I(x)$, where $I(x)=1$, and the first non-negative derivative is of the form $d^{2k+1}I/dx^{2k+1}$ for some integer $k \geq 1$.

(b) *Class 2*: critical points of $I(x)$, where $I(x)=0$, and the first non-negative derivative is of the form $d^{2k+1}I/dx^{2k+1}$ for some integer $k \geq 1$.

(c) *Class 3:* critical points of $I(x)$, which are local extrema but do not satisfy conditions (a) or (b).

The second step in the algorithm deals with the recovery of the phase-lead distribution. The phase-lead distribution can be reconstructed using the following formula:

$$p(x)=-2\pi M-(-1)^{M+N}2\arcsin\sqrt{I(x)}, \tag{9}$$

where $M \rightarrow M+(-1)^K$.

The algorithm starts with $M=0$, $N=0$, and $K=0$. The phase-lead distribution is recovered point-by-point increasing x from $-l/2$ to $l/2$. When a *Class 3* critical point is encountered, K is increased by one; when a *Class 2* critical point is encountered, N is increased by one; and, when a *Class 1* critical point is encountered, M is increased or decreased by one depending on the value of K.

One of the major problems with this algorithm is the need for analytical expressions for the light-intensity in order to calculate the high-order derivatives with accuracy. However, measurements of the light-intensity distribution are subject to noise quantization error and sampling that makes the calculation of derivatives impossible to the extent required by the algorithm. If the high-order derivatives cannot be calculated, then the classification of the critical points cannot be performed accurately, and the inverse problem of finding the phase-lead distribution becomes ill-posed.

4. PHASE-LEAD RECOVERY UNDER NON-IDEAL CONDITIONS

In this section, it is assumed that the output light of the polaridoscope is detected by a CCD linear array, mounted parallel to the x-coordinate, whose active length is the same as the transducer's. Since the linear array samples the light-intensity distribution in the pixel-quantized space, Equation (5) can be re-written in a discrete form as:

$$I(x_i)=\sin\frac{p(x_i)}{2} \qquad \text{for } i=1,2,...m, \quad (10)$$

where m is the number of pixels on the linear array. Note that, in Section 2, the light-intensity distribution was calculated for only 201 points. When $m>201$, the light-intensity values can be interpolated based on the values obtained using FEA.

The equations for $p(x)$ and $\psi_j(x)$, (3) and (4) respectively, can also be re-written in a discrete form as:

$$P_i = p(x_i) \qquad \text{for } i=1,2,...m \quad (11)$$

$$\Psi_{ij} = \Psi_j(x_i) \qquad \text{for } i=1,2,...m\,;\ j=1,2...n. \quad (12)$$

The discrete version of (3) can, thus, be re-written using a matrix notation as:

$$\boldsymbol{P}=\frac{1}{W}\Psi\,\boldsymbol{F}, \quad (13)$$

where

$$\boldsymbol{P}=\begin{bmatrix} P_1 \\ P_2 \\ \vdots \\ P_m \end{bmatrix};\ \Psi=\begin{bmatrix} \Psi_{11} & \Psi_{12} & \cdots & \Psi_{1n} \\ \Psi_{21} & \Psi_{22} & \cdots & \Psi_{2n} \\ \vdots & \vdots & & \vdots \\ \Psi_{m1} & \Psi_{m2} & \cdots & \Psi_{mn} \end{bmatrix};\ \boldsymbol{F}=\begin{bmatrix} F_1 \\ F_2 \\ \vdots \\ F_n \end{bmatrix}. \quad (14)$$

Herein, $\boldsymbol{P}$ is the phase-lead vector, Ψ is the base matrix, and $\boldsymbol{F}$ is the input force-profile vector. A relation similar to (14), but between strains and forces, has been reported for the case of piezo-resistive tactile transducers.[16,20]

Once the light-intensity has been discretized by the linear array, the measurements are converted into digital form by an A/D converter. The A/D converter introduces quantization errors in addition to the random electronic noise that would be present due to the detection process. The detected light-intensity distribution (in grey levels), I_d, can be written as:

$$I_d(x_i) = round\left[A\sin^2\frac{p(x_i)}{2} + n_o(x_i) + I_o \right] \text{ for } i=1,2...m, \quad (15)$$

where n_o is the total noise introduced into the measurement; I_o is the minimum average voltage applied to the A/D converter, such that $[I_o + \min(n_o)] \geq 0$; and A is the maximum allowed dynamic range of the A/D converter, such that $[A + I_o + \max(n_o)] \leq 2^B - 1$, (where B is the number of bits in the A/D converter). The function $round(\cdot)$ returns the closest integer to the real number $(\cdot)$.

Now, the phase-lead distribution has to be recovered from (15). However, the critical points of I_d cannot be classified using the algorithm outlined in Section 3 since the derivatives of I_d would be zero or infinite. As a consequence, a new algorithm must be developed through which to invert the problem. The proposed algorithm is explained herein via the example used in the previous sections.

Let the light-intensity distribution be given by (15), and $p(x)$ be calculated using (13). For the example, the parameters for the A/D converter and the linear array are as follows: B=8 bits, m=2048, I_o=5 and A=245. The noise is assumed to be random and limited between -5 and 5 grey levels. Fig. 9, shows the noisy light-intensity distribution.

A description of the algorithm follows:

(a) The light-intensity distribution shown in Fig. 9 is filtered with an ideal low-pass filter. The noise, in our example, was reduced to the range of -2 to 2 grey levels (from -5 to 5) by utilizing a pass-band of 10 μm^{-1}.

(b) The filtered light-intensity distribution is normalized, Fig. 10, and the critical points are identified. In our example, they are c_k, $k=1, 2,...19$.

(c) Three regions exist in the normalized light-intensity distribution for the classification of the critical points, Fig. 10. In our example, on the normalized intensity scale, Region 1 is defined as $0.98 \leq I \leq 1$, Region 2 as $0 < I < 0.02$ and Region 3 as $0.02 \leq I \leq 0.98$. The widths of Regions 1 and 2 were obtained approximately by dividing the maximum error in the filtered light-intensity distribution by A (that is, 4/245~0.02). The critical points are now classified as follows:

(i) All *local extrema* in Region 1 are either *Class 1* or *Class 3* points (following the classification used in Section 3). In our example, c_3 and c_{17} are in Region 1.

(ii) All *local extrema* in Region 2 are either *Class 2* or *Class 3* points. In our example, c_{12} is in Region 2.

(iii) All *local extrema* in Region 3 are *Class 3* points. In our example, with the exception of c_3, c_{12} and c_{17} the rest of the points are in Region 3.

Due to uncertainty about the class of critical points in Regions 1 and 3, several different phase-lead distributions can be recovered using the algorithm outlined in Section 3, of which only one is correct. This constitutes an *ill-posed inverse problem.* Each local extremum in Regions 1 and 2 would yield two possible phase-lead distributions. If the total number of local extrema in Regions 1 and 2 is C, then the total number of possible phase-lead distributions is 2^C. In our example C=3, leading to 8 possible phase-lead distributions. For coding purposes, the number "1" is assigned to *Class 1*, "-1" to *Class 2* and "0" to *Class 3.* Table II.

(d) The number of possible phase-lead distributions is minimized. To accomplish this objective, all the possible cases are checked with respect to a set of verification rules:

Rule 1: If c_{k1} and c_{k2} are both *Class-1* or both two *Class-2* points, such that between them only *Class 3* critical points exist, then the number of Class 3 critical points must be odd. In our example, all the cases satisfy this Rule.

Rule 2: If c_{k1} is a *Class-1* (*Class-2*) point and c_{k2} is *Class-2* (*Class-1*) point such that between them only *Class-3* critical points exist, then the number of *Class-3* critical points must be even. In our example, all the cases satisfy this Rule.

Rule 3: The parameter M in (9) must be zero for $x = -l/2$ and $x = l/2$ since the following boundary conditions apply to the transducer: $p(-l/2)=p(l/2)=0$. * For instance, in our example, Cases 2, 4, 5, 7 and 8 do not satisfy this rule.

After applying the rules to our example, the possible set of phase-lead distributions was reduced to 3 (Cases 1, 3 and 6).

(e) The phase-lead distributions are reconstructed for the reduced set at hand.

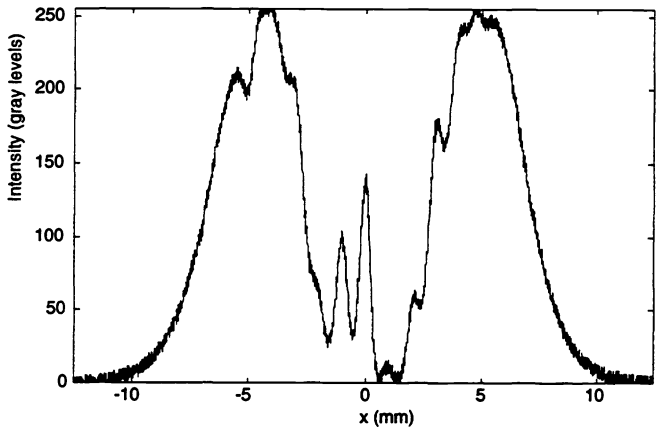

Fig. 9. Detected light-intensity distribution in grey levels.

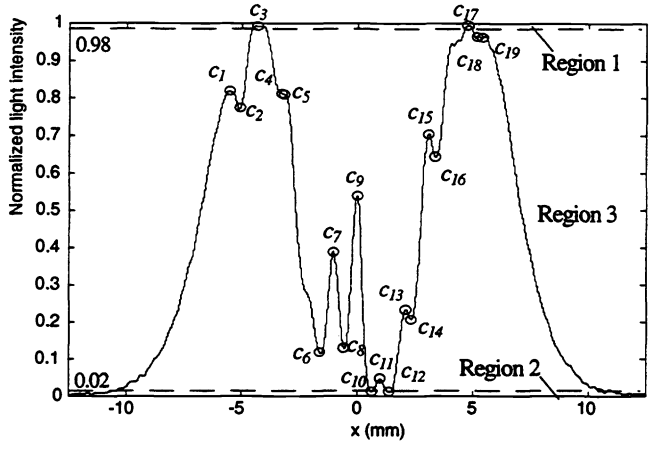

Fig. 10. Normalized filtered light-intensity distribution.

Table II: Complete set of possible critical points.

Case #	c_1	c_2	c_3	c_4 *to* c_{11}	c_{12}	c_{13} *to* c_{16}	c_{17}	c_{18}	c_{19}
1	0	0	0	0	0	0	0	0	0
2	0	0	0	0	0	0	1	0	0
3	0	0	0	0	-1	0	0	0	0
4	0	0	0	0	-1	0	1	0	0
5	0	0	1	0	0	0	0	0	0
6	0	0	1	0	0	0	1	0	0
7	0	0	1	0	-1	0	0	0	0
8	0	0	1	0	-1	0	1	0	0

* In our simulation, due to numerical errors in determining the stresses using FEA, $p(-l/2)$ and $p(l/2)$ are non-zero small negative values, however, this does not affect the value of M at the borders since $p(-l/2) > -\pi$ and $p(l/2) > -\pi$.

(f) Since only one of the solutions in the reduced set is the one sought, the spurious phase-lead distributions are eliminated.

To achieve this objective, in general, all the force-profiles, F_r, corresponding to the limited set of potential phase-lead distributions, P_r, must be found. One could be tempted to use (13) to find F_r, but it is realized that (13) can only be used for the forward analysis because the base matrix Ψ (a set of noise-free phase-lead distributions) cannot be determined from noisy measurements. Because of that we will have to determine F_r by solving the following expression:

$$P \cong \frac{1}{W}\hat{\Psi}\, F_r \,. \tag{16}$$

where $\hat{\Psi}$ is the noisy base-matrix. This matrix can be found alternatively by applying a force W to each tactel such that the phase-lead distribution in all points is larger than $-\pi$; for our case W=0.4 N. Then, using (9), a noisy light-intensity distribution is obtained for each case. These noisy light intensities are filtered with the same filter used in Step (a) of the algorithm and then are normalized. Since the phase-lead distribution is larger than $-\pi$, the elements of each column of $\hat{\Psi}$ can be obtained using (6).

Then, F_r has to be found from (16). A similar problem was addressed in a previous study for the case of a piezoresistive tactile sensor.[20] Therein, a neural network was proposed to solve the inverse-tactile problem. In our case, the following non-negative least-squares problem was formulated and solved,

$$\min_{F_r} \left\| \frac{1}{W}\hat{\Psi}\, F_r - P_r \right\| , \qquad \text{such that } F_r \geq 0, \tag{17}$$

where $\hat{\Psi}$ and F_r are the coefficients of the objective function. The vector F_r is restricted to be non-negative due to the positive force profile requirement in our case.

In our example, for Case 1 in Table II, the following force profile was recovered using (17):

$$F_r = (0.2469, 0.0745, 0.0501, 0, 0, 0, 0, 0, 0, 0.1258, 0.2336)\ \text{N}$$

The recovered force profile obtained by (17) must be verified via (16). Let P_v be the phase-lead distribution obtained when the estimated force profile F_r is applied to (10):

$$P_v \cong \frac{1}{W}\hat{\Psi}\, F_r \,. \tag{18}$$

For the correct guess for P_r the difference between P_r and P_v must be minimal.

Let a normalized error be defined, for each case, as:

$$Error(\%) = \frac{1}{\Delta P_{max}} \max\{abs[P_v - P_r]\} \times 100, \tag{19}$$

where the function *abs* calculates the absolute value of each component of the difference between P_r and P_v, and ΔP_{max} is the difference between the overall absolute maximum and the overall absolute minimum of P_r and P_v.

In Fig. 11, both P_r and P_v are plotted for Case 1. As can be observed, there exists a large difference between the two phase-lead distributions. This correctly implies that Case 1 is not the true phase-lead distribution. The large difference between P_r and P_v is associated with the fact that, in the ideal (noise-free) case, the vector P_r would not be a linear combination of the ψ functions.

For Case 3, the corresponding P_r and P_v are shown in Fig. 12. Once again, it is noted that Case 3 is not the true phase-lead distribution. The corresponding force profile F_r associated with this case is:

$$F_r = (0.2359, 0.0835, 0.0679, 0, 0, 0, 0, 0, 0, 0)\ \text{N}$$

The correct phase-lead distribution is the one that corresponds to Case 6, Fig. 13. The normalized error for this case is 3.6% (Table III, shows the normalized error for all three cases considered). The recovered force profile for Case 6 is:

$$F_r = (0.0999, 0.0572, 0.1008, 0.0715, 0.2105, 0.2998, 0.1186, 0.1298, 0.1503, 0.1098, 0.0899)\ \text{N}.$$

When one compares the above F_r with the true input (see Fig. 4), the maximum error in any component is determined to be less than 3%.

Table III: Normalized Errors.

Case #	*1*	*3*	*6*
Error (%)	41.4	51.4	3.6

5. CONCLUSIONS

In this paper, a photoelastic tactile sensor has been studied using FEA to determine the stress distribution, and the theory of photoelasticity for the calculation of the phase-lead distribution. The developed technique allows one to take into account the effect of the boundary conditions on the phase-lead distribution of the transducer, creating as a consequence a more reliable model for the transducer.

The recovery of the phase-lead distribution from an ideal (noise-free) light-intensity distribution has been presented and used to help in the understanding of the ill-posed conditions that may be found when the phase-lead distribution must be recovered from a noisy light-intensity distribution. For the later case, a general algorithm has been presented for the automatic recovery of the phase-lead distribution. In this process, the noisy light-intensity distribution is assumed to be detected by a CCD array camera linked to an A/D converter. The algorithm tackles the ill-posed condition of the problem by reducing the set of possible phase-lead distributions and by checking physical properties of the solution. Some simulation results using a 2-D opto-mechanical finite-element model of the transducer have been presented to demonstrate the proposed algorithm. To solve the inverse tactile problem, an optimization function was successfully implemented.

In practice, finding the correct phase-lead distribution might be computationally time-consuming if each distribution is considered sequentially. This is a consequence of the complexity of the algorithm by which the inverse-tactile problem must be solved. However, it is quite possible to process the different phase-lead distributions in a parallel manner: Use of dedicated hardware to solve the inverse-tactile problem, such as the scheme proposed by Pati,[20] for instance, is particularly attractive.

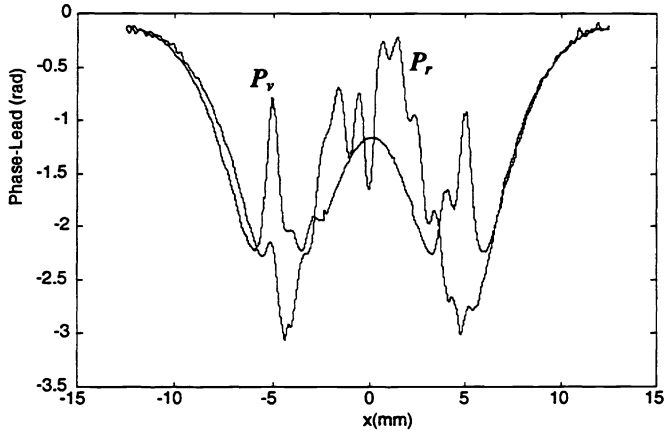

Fig. 11. Phase-lead distributions P_r and P_v for Case 1

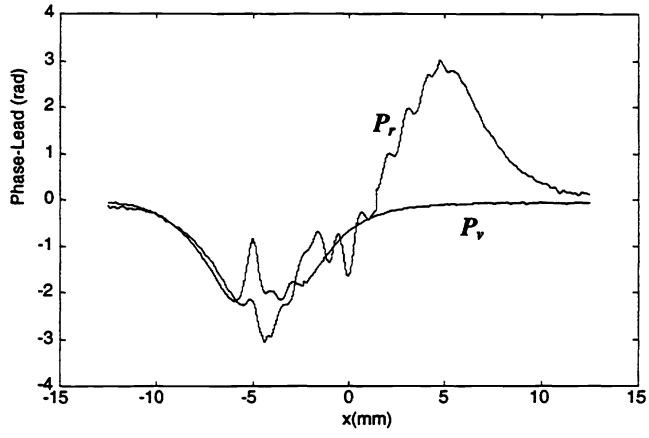

Fig. 12. Phase-lead distributions P_r and P_v for Case 3.

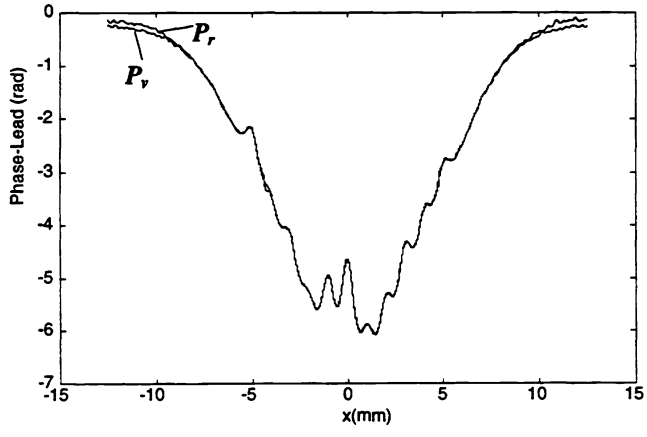

Fig. 13. Phase-lead distributions P_r and P_v for Case 6.

6. ACKNOWLEDGMENTS

The authors are grateful for the financial support provided by the Natural Sciences and Engineering Research Council of Canada. Mr. Saad would also like to thank CNPq, Brazil, for its financial support. Further, the authors would like to thank Dr. Tom Zougas for the development of the FEA programs and Mr. Dimiter Zlatanov for his comments on Section 3 of this paper.

APPENDIX I

The recovered phase-lead distribution, $\tilde{p}(x)$, given by:

$$\tilde{p}(x) = -2 \arcsin \sqrt{I(x)} \,, \tag{A.1}$$

can only provide the correct solution if the original phase-lead distribution $p(x)$ is larger or equal to $-\pi$ in the interval I=[-l/2 l/2]. If $p(x)$ is larger than -π in any sub-interval of I, then $\tilde{p}(x)$ is different than $p(x)$. For this case, $p(x)$ has sub-intervals where it is larger than -π. Then, $p(x)$ and $\tilde{p}(x)$ will have the same values in the sub-interval. Consider for example, the phase-leads in Fig. 8. As can be observed, the $p(x)$ and $\tilde{p}(x)$ have the same values in the interval $I_1 = \left[-l/2 \quad x_a\right]$, as well as in the interval $I_2 = \left[x_b \quad l/2\right]$.

Theorem: Let $p(x)$ be a linear combination of the linearly-independent functions $\psi_1(x)$, $\psi_2(x)$, ...$\psi_N(x)$ defined in the interval I=[-l/2 l/2]. Let us also assume that $\psi_1(x)$, $\psi_2(x)$, ...$\psi_N(x)$ are linearly independent in any open sub-interval of I. Let us now assume that a function $\tilde{p}(x)$ is identical to $p(x)$ in some, but not in all, open sub-intervals of I. Then, $\tilde{p}(x)$ is not a linear combination of the functions $\psi_1(x)$, $\psi_2(x)$, ...$\psi_N(x)$ in I.

Proof: Assume that $\tilde{p}(x)$ is a linear combination of $\psi_1(x)$, $\psi_2(x)$, ...$\psi_N(x)$ in I. Then, because of the additive property of linear functions, the function $p(x)$ - $\tilde{p}(x)$ should also be a linear combination of $\psi_1(x)$, $\psi_2(x)$, ...$\psi_N(x)$:

$$p(x) - \tilde{p}(x) = \sum_{i=1}^{N} \alpha_i \psi_i(x) \,. \tag{A.2}$$

In the sub-intervals of I where $p(x)$ and $\tilde{p}(x)$ are identical, the coefficients α_i must be *zero* since the theorem assumes that the functions $\psi_1(x)$, $\psi_2(x)$, ...$\psi_N(x)$ are linearly independent in any sub-interval of I. In the sub-intervals of I, where $p(x)$ and $\tilde{p}(x)$ are different, the coefficients α_i must be different than *zero*. Correspondingly, it is proven that the function $p(x)$ - $\tilde{p}(x)$ is not a linear combination of the functions $\psi_1(x)$, $\psi_2(x)$, ...$\psi_N(x)$ in I. Since, by definition, $p(x)$ is a linear combination of $\psi_1(x)$, $\psi_2(x)$, ...$\psi_N(x)$ in I, then, $\tilde{p}(x)$ cannot be linear combination of $\psi_1(x)$, $\psi_2(x)$, ...$\psi_N(x)$ in I.

7. REFERENCES

1. H. R. Nicholls and M. H. Lee, "A Survey of Robot Tactile Sensing Technology," *The International Journal of Robotics Research*, Vol. 8, No. 3, 1989, pp. 3-30.
2. R. A. Russell, *Robot Tactile Sensing*, Prentice Hall, Brunswick, 1990, 174 pages.
3. Ed. H.R. Nicholls, *Advanced Tactile Sensing for Robotics*, World Scientific Publishing Co. Pte. Ltd., Singapore, 1992, 294 pages.
4. S. Sugiyama, K. Kawahata, H. Funabashi, M. Takigawa and I. Igarashi, "A 32× 32 (1k)-Element Silicon Pressure-Sensor Array with CMOS Processing Circuits," *Electronics and Communications in Japan*, Part 2, Vol. 75, No. 1, 1992, pp. 64-75.
5. A. Cameron, R. Daniel and H. Durrant-Whyte, "Tactile Geometry for Images and Normal," in *Tactile Sensing and the Photoelastic Tactile Sensor,* Tech. Rep. OUEL 1758/89, Department of Engineering Science, University of Oxford, Parks Road, Oxford, 1989, pp. 1-16.
6. K. W. Loh, H. Durrant-Whyte and R. Daniel, "A Photoelastic Tactile Sensor" Tech,. Rep. OUEL 1792/89. Department of Engineering Science, University of Oxford, Parks Road, Oxford, 1989.
7. A. Cameron, R. Daniel and H. Durrant-Whyte, "Touch and Motion," *IEEE, International Conference on Robotics and Automation*, Philadelphia, 1988, pp. 1062-1067.
8. L. D. Harmon, "Automated Tactile Sensing," International Journal of Robotics Research, Vol. 1, No. 2, 1982, pp. 3-32.
9. S. C. Jacobsen, J. E. Wood, D. F. Knutti, and B. Biggers, "The Utah/MIT Dextrous Hand: Work in Progress," *Robotics Research: The First International Symposium,* Ed. M. Brady and R. Paul, The MIT Press, Cambridge, 1983, pp. 601-653.
10. F. Eghtedari and C. Morgan, "A Novel Tactile Sensor for Robot Applications", *Robotica*, Vol. 7, 1989, pp. 289-295.

11. S. H. Hopkins, F. Eghtedari and D. T. Pham, "Algorithms for Processing Data from a Photoelastic Slip Sensor," *Mechatronics*, Vol. 2, No. 1, 1992, pp. 15-28.
12. P. S. Theocaris and E. E. Gdoutos, *Matrix Theory of Photoelasticity*, Springer-Verlag, Berlin, 1979, 352 pages .
13. R. E. Saad, B. Benhabib and K. C. Smith, "A Novel Photoelastic Tactile Transducer for Robotics", *SME, Fifth World Conference on Robotics Research*, Cambridge, Massachusetts, 1994, pp. 4.1-4.14.
14. R. E. Saad, A. Bonen, K. C. Smith, and B. Benhabib, "Distributed-Force Recovery for a Planar Photoelastic Tactile Sensor," *IEEE International Conference on Instrumentation and Measurements*, Waltham, Massachusetts, 1995, pp. 532-537.
15. K. Iizuka, *Engineering Optics*, Springer-Verlag, 2nd Ed., Germany, 1987.
16. R. S. Fearing and J. M. Hollerbach, "Basic Solid Mechanics for Tactile Sensing," *International Journal of Robotics Research*, Vol. 4, No. 3, 1985, pp. 40-54.
17. M. Shimojo, "Spatial Filtering Characteristic of Elastic Cover for Tactile Sensor," *IEEE International Conference on Robotics and Automation*, San Diego, CA, 1994, pp. 287-292.
18. R. E. Ellis and M. Qin, "Singular-Value and Finite-Element Analysis of Tactile Shape Recognition," *IEEE International Conference on Robotics and Automation*, San Diego, CA, 1994, pp. 2529-2535.
19. S. L. Ricker and R. E. Ellis, "2-D Finite-Element Models of Tactile Sensors," *IEEE International Conference on Robotics and Automation*, Atlanta, GA, 1993, pp. 941-947.
20. Y. C. Pati, *Neural Networks for Low Level Processing of Tactile Sensory Data*, Master's Thesis, Department of Electrical and Computer Engineering, University of Maryland, College Park, 1989.